IEEE Access
Multidisciplinary ⋮ Rapid Review ⋮ Open Access Journal

Received May 18, 2020, accepted June 2, 2020, date of publication June 12, 2020, date of current version July 20, 2020.

Digital Object Identifier 10.1109/ACCESS.2020.3002103

Turbulent Structure Function Analysis Using Wireless Micro-Thermometer

SHIYONG SHAO[1,2,3], FUQIANG QIN[4], QING LIU[1,2], MANMAN XU[1,2,5], AND XUELING CHENG[6]

[1]Key Laboratory of Atmospheric Optics, Anhui Institute of Optics and Fine Mechanics, Chinese Academy of Sciences, Hefei 230031, China
[2]Advanced Laser Technology Laboratory of Anhui Province, Hefei 230037, China
[3]Science and Technology on Solid-State Laser Laboratory, Beijing 100015, China
[4]School of Computer Science and Technology, Northwestern Polytechnical University, Xi'an 710029, China
[5]Science Island Branch of Graduate School, University of Science and Technology of China, Hefei 230031, China
[6]State Key Laboratory of Atmospheric Boundary Layer Physics and Atmospheric Chemistry, Institute of Atmospheric Physics, Chinese Academy of Sciences, Beijing 100029, China

Corresponding author: Shiyong Shao (shaoshiyong@aiofm.ac.cn)

This work was supported in part by the National Key Research and Development Plan from the Ministry of Science and Technology of China under Grant 2018YFC0213102, in part by the National Science Foundation of China under Grant 41475024, and in part by the Science and Technology on Solid-State Laser Laboratory Fund under Grant 6142404180302.

ABSTRACT Most of the application scenarios of techniques related to electromagnetic wave transmission of photoelectric system are located in the earth's atmosphere or through the atmospheric path. The electromagnetic wave will change state through the atmosphere when encounters the inhomogeneities of refractive index caused by turbulence. Optical turbulence causes degradation of beam quality and energy to laser transmission, and brings image deterioration to astronomical observation. The refractive index structure coefficient is an important parameter describing the turbulence strength. For visible and near infrared band, the refractive index structure coefficient mainly depends on temperature structure coefficient. Using the theory of Wheatstone bridge, the micro-thermometer is designed and self-developed. To avoid interference from human and buildings, the wireless control for the micro-thermometer is realized based on CC1100. The observation of turbulence strength of representative test point, for more than one month, is implemented at Yangmeikeng near the South China Sea. Compared to ultrasonic anemometer, there is a sensitive lower measurement limit of micro-thermometer whose effective refractive index structure coefficient of system noise is less than $10^{-18}\mathrm{m}^{-2/3}$. There is obvious 'Sombrero' structure diurnal variation of turbulence near South China Sea, whose strength is mainly brought out by buoyancy heat bubble in day, and by wind shear at night. Monin–Obukhov length is positive at night and negative in day, and the scaling exponent is near $-5/3$ for temperature power spectrum, which is similar to wind power spectrum except for periods when wind from inland. The diurnal variation and scaling exponent of power spectrum analysis indicate that the measurement range and the sample rate of micro-thermometer are enough to response the turbulence measurement encountered in most laser transmission and astronomical observation fields. The turbulence characteristics information gained from micro-thermometer measurement data analysis brings good reference to optimal design and operation for photoelectric system.

INDEX TERMS Refractive index structure coefficient, temperature fluctuation, sensitivity calibration, wireless control, Monin–Obukhov length, scaling exponent.

I. INTRODUCTION

Turbulence transports matter and energy between the earth's surface and the atmosphere, which is an important reason for the change of boundary layer state [1]–[4]. The transport capacity of turbulence is several orders of magnitude larger than that of molecular diffusivity [5], [6]. Atmospheric optical turbulence is detrimental to ground-based photoelectric systems. The electromagnetic waves will change state through the atmosphere when encounter the inhomogeneities of refractive index caused by the atmospheric turbulence [7], [8], which is a thorny problem inducing scintillation [9], [10], beam wandering [11], [12], and wavefront aberration [13]–[15] especially to high energy laser as well as

The associate editor coordinating the review of this manuscript and approving it for publication was Stefania Bonafoni.

astronomical observation. Most of the application scenarios of various photoelectric technologies are located in the earth's atmosphere or through the atmospheric path. The system function will be affected by the atmospheric turbulence, and the probability of its effective use will be limited. It is of great significance to understand and master the optical properties of atmospheric turbulence, then correctly grasp the impact of atmospheric turbulence on the function of photoelectric system.

The strength of optical turbulence is usually described by the refractive index structure coefficient (C_n^2, $m^{-2/3}$) [16], [17]. Bufton *et al.* [18] measured turbulence in the troposphere by thermal sensor, then reduced its weight to less than 3 kg, and operated in only two scale ranges from a temperature difference noise level of 0.004 to a maximum temperature difference of $0.676K$ [19], [20]. Trinqueta *et al.* [21] presented in situ technique to measure the microstructure of the temperature field in atmosphere, which gained the structure function of refractive index along with atmospheric pressure, temperature, humidity, and wind speed. This cross-calibrated technique gave a higher spatiotemporal resolution than before. Mchugh and Sharman [22] measured optical turbulence over Mauna Kea on the island of Hawaii using thermosondes suspended from ascending balloons. The results showed good agreement with Differential Image Motion Monitor(DIMM), although the thermosonde underpredicted the seeing at the summit since ground layer turbulence unable to be counted.

In present, there are also a variety of model methods to estimate C_n^2 [16], [23], such as Mesoscale Non-hydrostatic (Meso-Nh) model, Numerical Weather Prediction (NWP) model etc., but their results inevitably have some calculation errors since premises exist, so the calculation precision needs verification from exploration. The atmospheric exploration requires high-precision scientific instruments [24], [25], meanwhile, the development of observation instruments has also promoted the progress of atmospheric science theory, numerical model and simulation, and its importance has been confirmed by the development of atmospheric science [26]. Direct detection by instruments is still the most basic and reliable method for turbulence study. The turbulence strength detection using the ultrasonic anemometer is an often reported method [27], [28].

Although a lot of work has been done on atmospheric optical turbulence, the analysis of turbulent power spectrum and turbulent power source is relatively lacking, so it is difficult to understand the development degree and stable state of turbulence in field site. Atmospheric turbulence is time-varying, and the measurement of its instantaneous strength is difficult to repeat. However, reliability and accuracy of measurement data should be verified to help us an insight into the physics of the optical turbulence. Therefore, it is necessary to synchronously measure using different principle instruments for mutual verification, and to gain the corresponding conclusion by comparative analysis of multi-source data.

Study on regularity of the refractive index structure coefficient needs a large number of measurement data, so the continual measurement is required, and for minimizing impact from buildings, human activities, etc., the measurement instruments are often be placed at representative open locations, so the wireless control to the measurement instrument is necessary for timely observation of measurement data. To visible and near infrared light waves, the fluctuation of atmospheric refractive index is mainly caused by temperature fluctuation [29],then the micro-thermometer based on temperature fluctuation is aimed and self-developed, then observations from a field campaign over Yangmeikeng implemented for validation of the instrument in the paper.

The rest of the paper is organized as follows: Section II discusses the influence factors and calculation of the refractive index structure coefficient, meanwhile, the design and wireless control of a micro-thermometer are introduced. The field campaign scene and instruments calibration are indicated in section III, then the main performance indexes of micro-thermometer and corresponding turbulence characteristics are given in section IV based on measurement data analysis. Section V concludes this paper.

II. BACKGROUND

A. REFRACTIVE INDEX STRUCTURE COEFFICIENT

Kolmogorov introduced the structure function to explore turbulence characteristics [30], [31]. Due to dimensional analysis, the turbulence spectra in the inertial-subrange conforms to "2/3" power law [32]. Fluctuation of the refractive index can be expressed as

$$D_n = \left\langle \left(n\left(\overrightarrow{x}\right) - n\left(\overrightarrow{x} + \overrightarrow{r}\right)\right)^2 \right\rangle = C_n^2 r^{2/3}, \quad l_0 \le r \le L_0 \tag{1}$$

where $\langle\rangle$ is the ensemble average, n is the refractive index of air, $\overrightarrow{x}$ and $\overrightarrow{r}$ indicate the position vector, r denotes the magnitude of $\overrightarrow{r}$, l_0 and L_0 are the inner and outer scales of the atmospheric turbulence.

To light wave and electromagnetic wave, the effect of humidity can be negligible, so the refractive index n can be written as a function of the atmospheric pressure P and Kelvin temperature T.

$$n - 1 = 79 \times 10^{-6} \frac{P}{T} \tag{2}$$

Above three parameters can be decomposed average term and fluctuation term, respectively written as $n = \overline{n} + \Delta n'$, $P = \overline{P} + \Delta P'$, $T = \overline{T} + \Delta T'$, so the fluctuation term of refractive index is

$$\Delta n' = 79 \times 10^{-6} \left(\frac{\Delta P'}{\overline{P}} - \frac{\Delta T'}{\overline{T}} \right) \frac{\overline{P}}{\overline{T}} \tag{3}$$

For the actual atmosphere, the fluctuation term of refractive index is mainly affected by temperature

$$\Delta n' = -79 \times 10^{-6} \frac{\overline{P}}{\overline{T}^2} \Delta T' \tag{4}$$

In actual operation, the average temperature and air press are not sudden variable characters, considering the convenience of expression, usually $\overline{T}$ and $\overline{P}$ written as T and P. So the refractive index structure coefficient C_n^2 can be defined as follows [33]–[35]

$$C_n^2 = \left(79 \times 10^{-6} \frac{P}{T^2}\right)^2 C_T^2 \tag{5}$$

where C_T^2 is the temperature structure coefficient. The calculation of C_T^2 involves the measurement of the square and average of the temperature difference given by two sensors which are separated by a known distance [36], [37]. As defined by Obukhov [38], the temperature structure coefficient C_T^2 for a Kolmogorov type spectrum is given by

$$C_T^2 = \langle (T(\overrightarrow{x}) - T(\overrightarrow{x} + \overrightarrow{r}))^2 \rangle r^{-2/3}, \quad l_0 \le r \le L_0 \tag{6}$$

According to Kolmogorov theory, Monin-Obukhov similarity theory and semi-empirical relationships of Wyngaard and Izumi [39], the refractive index structure coefficient can be obtained by meteorology factors from ultrasonic anemometer. By Talyor's turbulence freezing assumption, the spatial structure of turbulence can be analyzed by time series of turbulence, then the temperature structure coefficient C_T^2 can be expressed

$$C_T^2 = \left\langle \left[T'\left(\overrightarrow{x}\right) - T'\left(\overrightarrow{x} - Vt\right)\right]^2 \right\rangle (Vt)^{-2/3} \tag{7}$$

where T' is virtual temperature, V is horizontal wind speed, $t = r/V$ is the duration. The relationship between T' and T is $T' = T(1+0.3192e/P)$ [40], where e is water vapor pressure, in the paper, since test site close to South China sea surface, P is the standard atmospheric pressure 101hpa, and according to data analysis, e/P is no more than 0.3, so T' can be replaced by T approximately. The $V = \left(u^2 + v^2\right)^{1/2}$ is sum of radial wind speed u and transverse wind speed v, for ultrasonic anemometer used in the field campaign, the measurement range is 0m/s to 40m/s.

B. SELF-DEVELOPED MICRO-THERMOMETER

For measuring the refractive index structure coefficient rapidly and effectively, we self-develop the micro-thermometer, whose schematic diagram is displayed in below Fig.1(a). The two probes R_{T1} and R_{T2} are legs of a Wheatstone bridge, and the resistance of probe is proportional to temperature, thus temperature changes are sensed as an imbalance voltage of the bridge [41]. Just as in Fig.1(b), the two temperature probes of micro-thermometer are made of platinum wires with $10\mu m$ diameter and mounted on opposing ends with 1m interval. Each temperature probe has a resistance wire with a time constant less than 2ms. The Wheatstone bridge can resolve temperatures as low as 0.001K. Compared to existing devices for turbulence strength measurement mentioned before, the micro-thermometer can remove the water drops on the platinum wires from precipitation by regular hot air purging, meanwhile, once

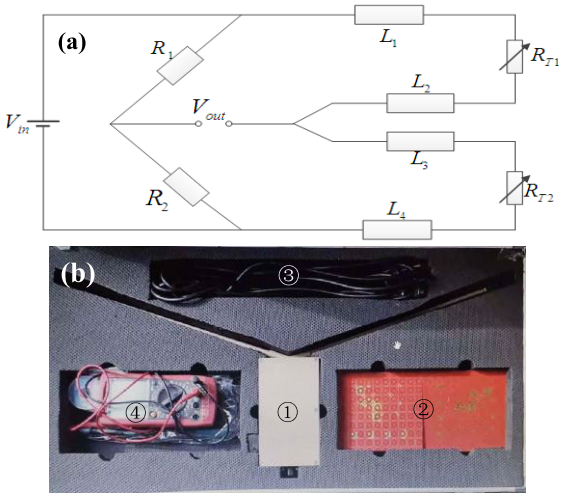

FIGURE 1. Schematic diagram(a) and instrument picture(b) of a micro-thermometer, ① micro-thermometer ② platinum wire box ③ power and signal wire ④ multi-meter.

the platinum wire breaks under the action of external force, an alarm will be given through the acquisition software immediately, and the plug-in probe with platinum wire can be replaced as soon as possible.

The temperature of sensor location is gained by measuring the resistance of platinum wire

$$R_T = R_{ref}[1 + \alpha\left(T - T_{ref}\right)] \tag{8}$$

where R_T is the resistance of platinum wire at Kelvin temperature T, R_{ref} is the resistance of platinum wire at reference Kelvin temperature T_{ref}, α is the temperature index. From $273K$ to $373K$, there is linear relationship between the resistance of platinum wire and its temperature. The constant $T_{ref} = 273K, \alpha = 3.85 \times 10^{-3}K^{-1}$.

In Fig. 1(a), setting the resistance $R_1 = R_2$, the equivalent resistance of circuit line $L_1 = L_2 = L_3 = L_4 = L$, so

$$\Delta T' = \frac{V_{out}}{V_{in}} \cdot \frac{2\left(R_{T1} + R_{T2} + 4L\right)}{R_{ref}\alpha} \tag{9}$$

where R_{T2} and R_{T1} are platinum wire resistance of sensing probes. Generally, input voltage V_{in} is $24V$, $\Delta T'$ can be calculated by output voltage V_{out}, then the C_n^2 is gained based on C_T^2.

A whole set of micro-thermometer is shown in Fig.1 (b). Since the platinum wire is easy to break due to external influence, 20 pairs platinum probes are equipped in a platinum wire box to ensure timely replacement. The power and signal wire is for power supply and signal transmission. Constant temperature treatment to the circuit has been done for minimum thermal noise, and the resistance difference $R_{T2} - R_{T1}$ needs be limited within 2Ω, which is realized by multi-meter, for realizing the temperature difference measurement sensitivity to $0.001K$, that is slightly lower than equivalent $10^{-18}m^{-2/3}$.

C. WIRELESS CONTROL

To avoid human and building interference, the field test point is often selected at an open farther space. The wireless control to the measurement instrument is usually preferred. In the following field campaign, wireless data communication system based on CC1100 was used [42]–[44]. The data through RS232 serial port is downloaded to microcontroller unit, then microcontroller unit control CC1100 used to realize the stable communication, and uploaded data sent to PC. The whole process is displayed in Fig.2.

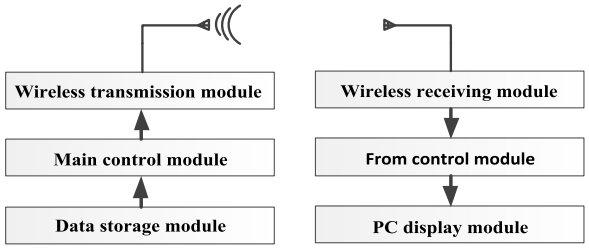

FIGURE 2. Schematic diagram of wireless control of the micro-thermometer.

III. FIELD CAMPAIGN

A. SELECTION OF TEST SITE

The field test point was selected at Yangmeikeng Ecology Center, a place close to the South China Sea and back on mountains in Shenzhen city in Guangdong province. The east side of a meteorological tower faces the South China Sea, and the micro-thermometer was installed on the side with an altitude of 130m above sea level. The location of the test site and the experimental scenario picture of micro-thermometer are shown in Fig. 3. The underlying surface of the test site was green vegetation with good typicality for turbulence measurement. The linear distance between micro-thermometer and the data receiving point was 120m. The test was implemented between late Aug. and middle Oct. in 2019, satisfied for data reliability from a statistical point of view, which relies on a large amount of observation data for a relative long time.

B. INSTRUMENT CALIBRATION AND COMPARISON

To ensure reliability and accuracy of the measurement data from micro-thermometer, we established a comparative verification. The UAT-3 ultrasonic anemometer, prepared by Institute of Atmospheric Physics, Chinese Academy of Sciences, was placed 1m horizontal interval away self-developed QHTP-2 micro-thermometer and measured synchronously. For evaluating the measurement sensitivity of micro-thermometer, we designed an up to 90 hours of comparative measurement to the system noise between micro-thermometer and ultrasonic anemometer, whose result shown in Fig.4. The sample rate is 30Hz and 100Hz for micro-thermometer and ultrasonic anemometer respectively. The data from the two instruments is averaged per minute. The system noises of micro-thermometer and ultrasonic

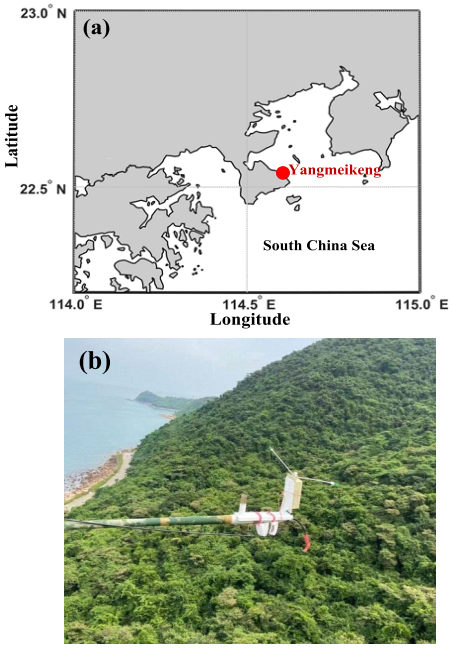

FIGURE 3. Location of test site(a) and scenario(b).

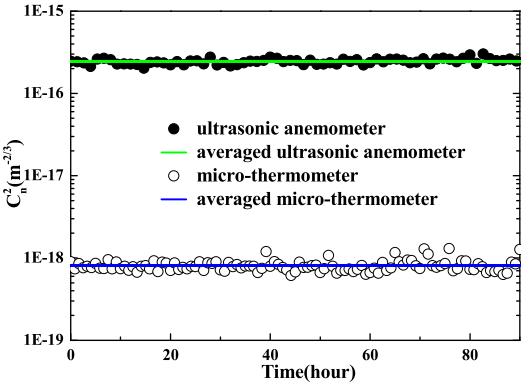

FIGURE 4. Effective C_n^2 of system noise of ultrasonic anemometer and micro-thermometer.

anemometer are all relatively stable. The averaged system noise effective C_n^2 of above two instruments are $8.17 \times 10^{-19} m^{-2/3}$ and $2.43 \times 10^{-16} m^{-2/3}$ respectively, which indicates the sensitivity of the micro-thermometer is far higher than that of the ultrasonic anemometer, and the former more advantageous for the measurement of weak turbulence. Considering SNR, the turbulence strength under $10^{-15} m^{-2/3}$ will be difficult to be detected effectively by ultrasonic anemometer.

IV. TEST RESULTS AND DISCUSSION

A. DIURNAL VARIATION

Since the turbulence strength is affected by weather for different solar radiation and earth surface thermal radiation, the refractive index structure coefficient C_n^2 should show different state as time goes on, that is, the diurnal variation maybe exist. By micro-thermometer and ultrasonic

anemometer, 1.7×10^4 and 8.64×10^6 groups measurement data are gained every day, respectively. Arithmetic averaged data per minute is used to analyze the diurnal variation, so the final averaged data of micro-thermometer and ultrasonic anemometer are all 1440 groups every day.

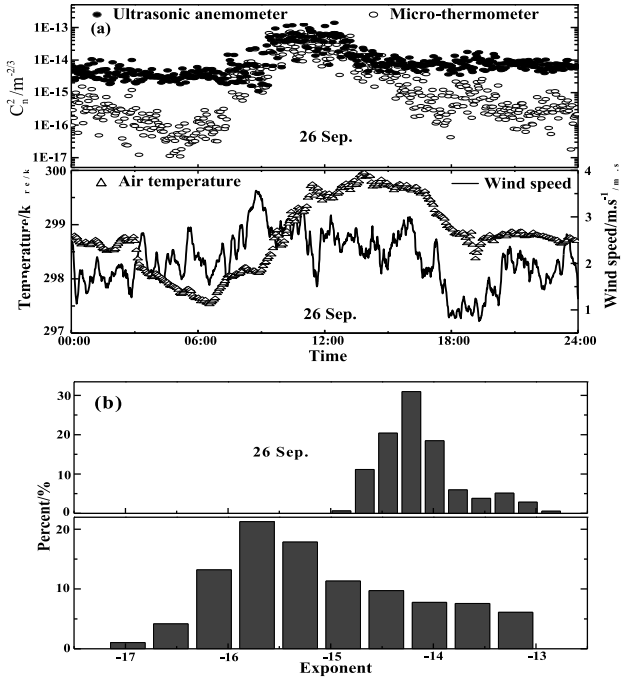

FIGURE 5. On 26 Sep., C_n^2 diurnal variation measured by micro-thermometer and ultrasonic anemometer, the synchronous air temperature and wind speed (a), corresponding proportion distribution of exponent of turbulence strength (b).

In Fig. 5, the result of 26 Sep. in 2019 is shown, a sunny day representing the majority of weather conditions in Shenzhen coast. The turbulence diurnal variation detected by ultrasonic anemometer and micro-thermometer all present 'Sombrero' structure shown in Fig.5(a) upper panel, the turbulence strength strong in day and weak at night. The time of weakest turbulence is customarily called 'conversion time' [45]. Conversion times of the day appear at around 6:00 and 18:00, corresponding to about half an hour at sunrise and sunset, respectively. The diurnal variation of air temperature and wind speed is also shown in Fig.5(a) lower panel. The temperature range is 297 K to 300 K, and the majority of wind speed is under $3m/s$. Since the range of temperature change is relative small and press is approximate equal to standard atmospheric pressure, the uncertainty in the equation (5) transform from C_T^2 to C_n^2 is negligible.

There is an obvious diurnal variation of temperature similar to turbulence strength except a certain time delay, but without apparent trend for the wind speed. Temperature gradient of day is more intensive than that of night. For turbulence above $10^{-14}m^{-2/3}$, there are similar response to ultrasonic anemometer and micro-thermometer, but micro-thermometer with higher sensitivity for turbulence under $10^{-15}m^{-2/3}$, which is also brought out from statistic of turbulence strength exponent range in Fig.5(b). For real atmosphere, the turbulence intensity under $10^{-15}m^{-2/3}$ accounts for a considerable proportion, therefore, compared with the ultrasonic anemometer, the micro-thermometer broadens the detection range of turbulence strength.

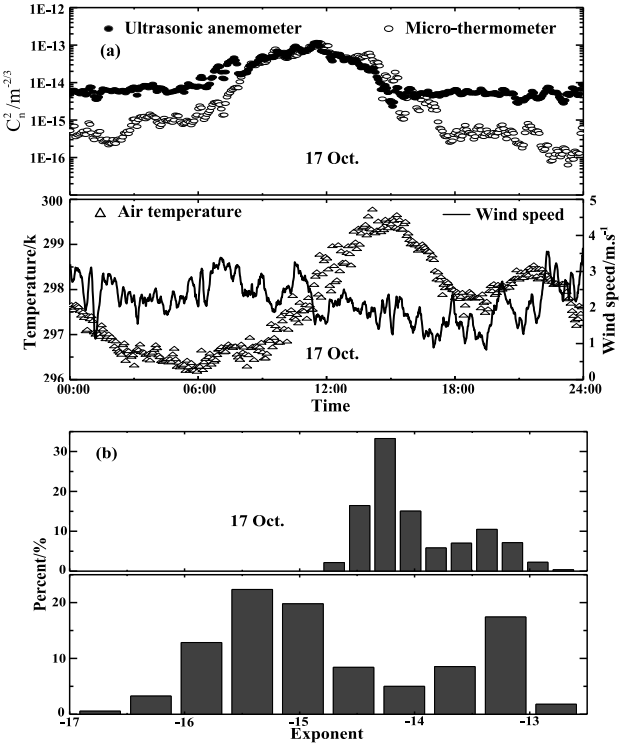

FIGURE 6. On 17 Oct., C_n^2 diurnal variation measured by micro-thermometer and ultrasonic anemometer, the synchronous air temperature and wind speed (a), corresponding proportion distribution of exponent of turbulence strength (b).

To verify the reliability of diurnal variation of measurement data, the other representative day, 17 Oct., is selected. The turbulence strength in Fig.6(a), no matter from ultrasonic anemometer or micro-thermometer, is generally stronger and smoother than that of 26 Sep., but conversion times are vague. The temperature range is $296K$ to $300K$, and the majority of wind speed is between $1m/s$ and $3m/s$ with relative stable wind speed shear. Temperature gradient of day is also significantly higher than that of night, meanwhile wind speed is generally stable, therefore the temperature gradient or heat bubble plays an important role in the development of day turbulence. The proportion distribution of exponent of turbulence strength in Fig.6(b) is similar to one in Fig.5(b), the large proportions of C_n^2 from micro-thermometer appear below $10^{-15}m^{-2/3}$ which is the upper limit of measurement accuracy for ultrasonic anemometer.

During the test period from Aug. to Oct., except rainy days and days with bad data, measurement data of 32 days are gathered to evaluate the monthly diurnal variation, in total 5.44×10^5 groups data from micro-thermometer, and 2.76×10^8 groups data from ultrasonic anemometer. Ultimately, the monthly diurnal variation of C_n^2 is gained by

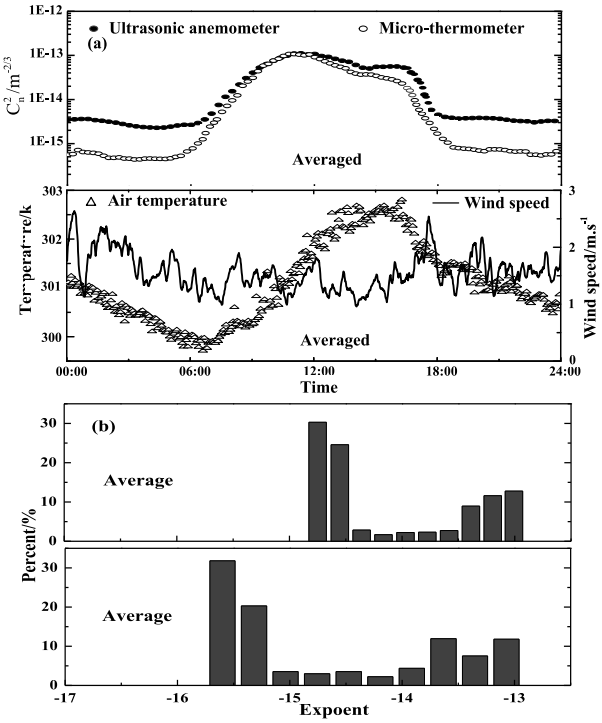

FIGURE 7. The monthly averaged diurnal variation of C_n^2 from micro-thermometer and ultrasonic anemometer, the synchronous air temperature and wind speed (a), and corresponding proportion distribution of exponent of turbulence intensity (b).

averaging per minute as shown in Fig.7(a) upper panel, and all display the smoother 'Sombrero' structure whose turbulence strength strong in day and weak at night. The monthly averaged C_n^2 diurnal variations are generally along the center line of single day, so the small proportion data under $1 \times 10^{-16} m^{-2/3}$ and other disorganized data disappear after arithmetic average. For micro-thermometer and ultrasonic anemometer, the developing trends of turbulence strength and the detection range are shown more clearly. The statistical response capability of micro-thermometer and ultrasonic anemometer to turbulence strength is displayed in Fig.7(b). The monthly averaged data of noon and night is a large proportion compared to the up and down periods between strong and weak turbulence. Similar to the diurnal variation of single day, the monthly averaged temperature gradient of day is also higher than that of night, and wind shear is also relative stable in Fig.7(a) lower panel.

B. MONIN–OBUKHOV LENGTH

Monin–Obukhov length is a parameter in the atmospheric boundary layer near the ground surface to characterize the relative contribution of wind shear stress and buoyancy to turbulent kinetic energy [46], [47].The Monin-Obukhov theory has been considered the backbone of surface layer meteorology [47]. Its definition is

$$L = \frac{-u_*^3 T_v}{kgQ_{vo}} \tag{10}$$

where u_* is friction velocity, T_v is the mean temperature of the surface layer in Kelvin, $k = 0.4$ is the Von Kármán constant, g is the acceleration of gravity, Q_{vo} is the temperature flux of near surface layer. The numerator represents energy from shear stress, the denominator represents energy from buoyancy or against gravity. L is positive when stable and negative when unstable. The lower the value is, the more stable ($L > 0$) or unstable ($L < 0$).

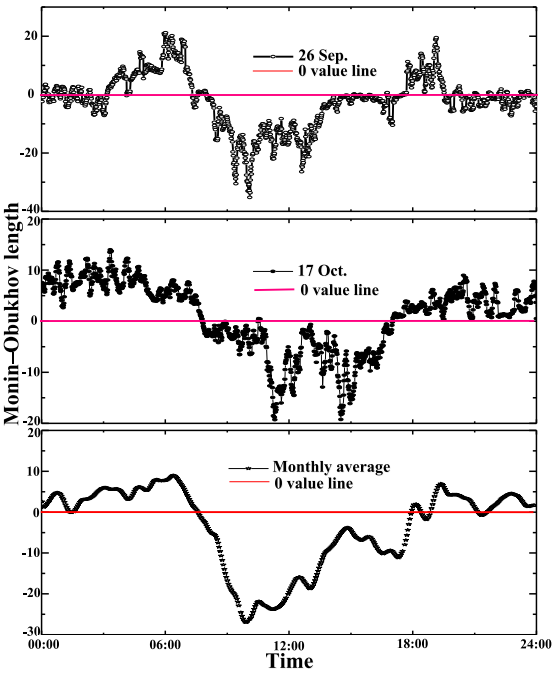

FIGURE 8. Diurnal variation of Monin–Obukhov length.

The daily and monthly averaged diurnal variation of Monin–Obukhov length is shown in Fig.8, both show instability in day and stability at night, and the conversion time just at dusk and dawn. As mentioned before, turbulence is brought out by buoyancy heat bubble and wind shear. Since the wind shear is evenly distributed in general whether it's night or day, temperature gradient in day is more intensive than at night due to buoyancy heat bubble in day from solar radiation and underlying surface thermal radiation, so the instability of Monin–Obukhov length is mainly from buoyancy heat bubble. The underlying surface is cooler than the air temperature in night, then the thermal inversion layer is formed and Monin–Obukhov length changes to stable positive value. Turbulence strength is driven to some extent by temperature gradients, and during crossover the gradients drop to near zero and therefore so does C_n^2.The monthly averaged temperature and wind speed all display homologous diurnal variation with the single day, so the buoyancy heat bubble from solar radiation is the main source of intensive turbulence in day is further confirmed from a statistical point of view. Above results elaborate the 'Sombrero' structure of the diurnal variation of C_n^2.

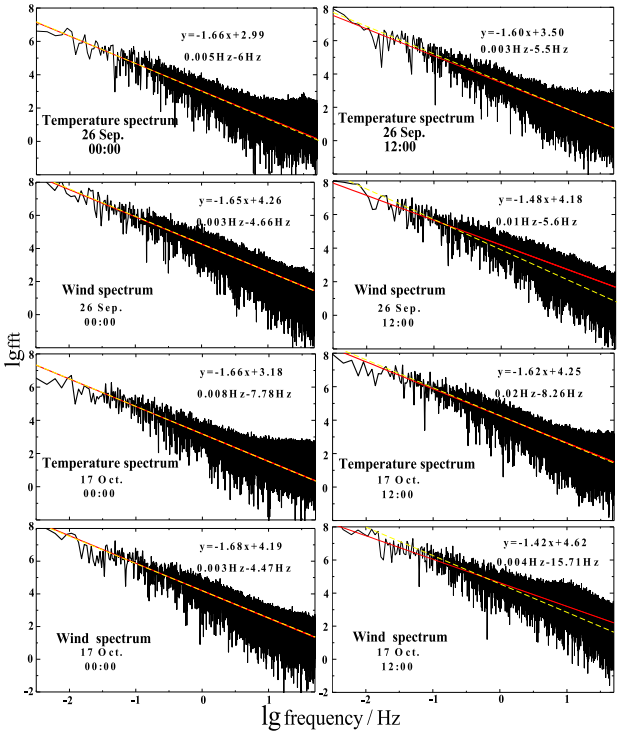

FIGURE 9. Scaling exponent of temperature/wind power spectrum, linear fitting plotted by red line and −5/3 line plotted by yellow dotted line at representative times.

C. SCALING EXPONENT OF POWER SPECTRUM

Power spectrum is usually used to characterize the statistical characteristics of turbulence in laser atmospheric transmission and astronomical observation. By decomposing frequency and power spectrum, we can find the role of turbulence vortices of different time and space scales in turbulence. After Fourier transform to the measured temperature and wind speed time series, the power spectrum $W(f)$ is obtained, then logarithmic operation is performed, finally, the intercept α and the slope β are gained by linear fitting in the inertial-subrange [49]

$$\lg[W(f)] = \alpha + \beta \lg(f) \tag{11}$$

where β is the scaling exponent of power spectrum.

The temperature and wind power spectrum on 26 Sep. and 17 Oct. in 2019 is analyzed at two representative time points 00:00 and 12:00. The −5/3line is plotted by yellow dotted line in each panel for the convenience of comparison with the ideal situation. The scaling exponents of temperature power spectrums are all around −5/3, but the scaling exponents of wind power spectrum display different results, which close to −5/3 at night but deviate from −5/3 during the day, illustrating the development of buoyancy heat bubble is sufficient, meanwhile, the development of wind shear is affected by source with different underlying surface such as sea or inland. In a word, the development degree of turbulence in inertial subrange from sea wind at night is more ergodic and complete developed compared to one from inland wind during the day. The linear fitting formulas are written to respective power spectrums, and the frequency ranges, less than 10Hz in most cases, also listed under each fitting formulas.

By repeated and comparative tests for more than one month, the main indexes of micro-thermometer are verified to achieve design objectives. The sample frequency and measurement range are introduced in below Table 1, meanwhile, the same indexes of ultrasonic anemometer also exhibited. The energy is mainly included in low frequency turbulence, and turbulence strength suitable for laser transmission and astronomical observation rarely exceeds $10^{-12}m^{-2/3}$, so the 0.1Hz to 30Hz sample frequency and $10^{-18}m^{-2/3}$ to $10^{-12}m^{-2/3}$ measurement range of micro-thermometer are satisfied for turbulence measurement. The sample frequency range of ultrasonic anemometer broadens the turbulence spectrum analysis ability. The measurement range of optical turbulence spans $10^{-15}m^{-2/3}$ to $10^{-12}m^{-2/3}$, containing turbulence with strength above medium, which brings out an important verification method.

TABLE 1. Main indexes of measuring instruments.

Measuring instrument	Sample Frequency (Hz)	Measurement range ($m^{-2/3}$)
micro-thermometer	0.1 to 30	10^{-18} to10^{-12}
ultrasonic anemometer	10 to 100	10^{-15} to10^{-12}

V. CONCLUSION

Most of the transmission paths of the photoelectric system pass through the atmosphere, and optical turbulence is always the inevitable factor causing degradation of transmission performance. The refractive index structure coefficient is a parameter for describing the turbulence strength. Using the approximate linear relationship between the refractive index structure function and the temperature structure coefficient, the micro-thermometer based on a Wheatstone bridge is designed and self-developed. The wireless control is implemented to avoid external interference at representative test points. By analyzing measurement data of the Yangmeikeng field campaign over one month, there are similarity of diurnal variation from micro-thermometer and ultrasonic anemometer of single day and monthly averaged, however, the micro-thermometer has a sensitive lower measurement limit. The diurnal variation of Monin–Obukhov length indicates that the turbulence only from wind shear at night, and from buoyancy heat bubble and wind shear during the day, which proves that the buoyancy heat bubble is the main source causing Monin–Obukhov length negative. Based on scaling exponent analysis of temperature and wind power spectrum, the development extent of turbulence in inertial subrange from sea wind at night is more ergodic and complete compared to one from inland wind during the day. The results from field campaign indicate that the sample rate and measurement range of micro-thermometer are enough to response the turbulence encountered in most laser transmission and

astronomical observation fields. The measurement data of wireless micro-thermometer brings good reference to optimal design and operation for photoelectric system.

REFERENCES

[1] M. Pahlow, M. B. Parlange, and F. Porté-Agel, "On Monin–Obukhov similarity in the stable atmospheric boundary layer," *Boundary-Layer Meteorol.*, vol. 99, no. 2, pp. 225–248, May 2001.

[2] J. Liang, L. Zhang, Y. Wang, X. Cao, Q. Zhang, H. Wang, and B. Zhang, "Turbulence regimes and the validity of similarity theory in the stable boundary layer over complex terrain of the loess plateau, China," *J. Geophys. Res. Atmos.*, vol. 119, no. 10, pp. 6009–6021, May 2014.

[3] X. Hu, P. M. Klein, and M. Xue, "Evaluation of the updated YSU planetary boundary layer scheme within WRF for wind resource and air quality assessments," *J. Geophys. Res. Atmos.*, vol. 118, no. 18, pp. 10490–10505, 2013.

[4] H. Dekker, G. de Leeuw, and A. Maassen van den Brink, "Boundary-layer turbulence as a kangaroo process," *Phys. Rev. E, Stat. Phys. Plasmas Fluids Relat. Interdiscip. Top.*, vol. 52, no. 3, pp. 2549–2558, Sep. 1995.

[5] H. Zhou and X. Wu, "A wind tunnel investigation and numerical modeling on turbulence flow in street canyons," *Acta Aerodynamica Sinica*, vol. 16, no. 4, pp. 411–418,1998.

[6] I. Y. Lee and H. M. Park, "Parameterization of the pollutant transport and dispersion in urban street canyons," *Atmos. Environ.*, vol. 28, no. 14, pp. 2343–2349, Aug. 1994.

[7] D. L. Fried, G. E. Mevers, and M. P. Keister, "Measurements of laser-beam scintillation in the atmosphere," *J. Opt. Soc. Amer.*, vol. 57, no. 6, pp. 787–797, 1967.

[8] T. Chiba, "Spot dancing of the laser beam propagated through the turbulent atmosphere," *Appl. Opt.*, vol. 10, no. 11, pp. 2456–2461, 1971.

[9] N.-N. Zhang, S. Xin, Z. Yan-Ge, F. Yang, and G. Song, "Simulated experiment of the light intensity influenced by non-Kolmogorov turbulence," *Acta Photonica Sinica*, vol. 47, no. 8, pp. 0601002-1–0601002-9, 2018.

[10] D. L. Fried, G. E. Mevers, and M. P. Keister, "Measurements of laser beam scintillation in the atmosphere," *J. Opt. Soc. Amer.*, vol. 57, no. 6, pp. 787–797, 1967.

[11] X. Huang, S. Nan, W. Tan, Y. Bai, and X. Fu, "Statistical properties of Gaussian Schell-model beams propagating through anisotropic hypersonic turbulence," *OSA Continuum*, vol. 2, no. 12, pp. 3584–3597, 2019.

[12] D. L. Walters, "Measurements of optical turbulence with higherorder structure functions," *Appl. Opt.*, vol. 34, no. 9, pp. 1591–1597, 1995.

[13] H. Mei, B. Li, H. Huang, and R. Rao, "Piezoelectric optical fiber stretcher for application in an atmospheric optical turbulence sensor," *Appl. Opt.*, vol. 46, no. 20, pp. 4371–4375, 2007.

[14] R. Rao, "Science and technology of atmospheric effects on optical engineering: Progress in 3rd quinquennium of 21st century," *Sci. China Technol. Sci.*, vol. 60, no. 12, pp. 1771–1783, Dec. 2017.

[15] L. Cui, B. Xue, and F. Zhou, "Atmospheric spectral model and theoretical expressions of irradiance scintillation index for optical wave propagating through moderate-to-strong non-Kolmogorov turbulence," *J. Opt. Soc. Amer. A, Opt. Image Sci.*, vol. 33, no. 4, pp. 483–491, 2016.

[16] R. Avila, J. Vernin, and E. Masciadri, "Whole atmospheric-turbulence profiling with generalized Scidar," *Appl.Opt.*, vol. 36, no. 30, pp. 7898–7905,1997.

[17] M. Sarazin and F. Roddier, "The ESO differential image motion monitor," *Astron. Astrophys.*, vol. 227, no. 1, pp. 294–300, 1990.

[18] J. L. Bufton, P. O. Minott, M. W. Fitzmaurice, and P. J. Titterton, "Measurements of turbulence profiles in the troposphere," *J. Opt. Soc. Amer.*, vol. 62, no. 9, p. 1068, Sep. 1972.

[19] J. L. Bufton, R. S. Iyer, and L. S. Taylor, "Scintillation statistics caused by atmospheric turbulence and speckle in satellite laser ranging," *Appl. Opt.*, vol. 16, no. 9, pp. 2408–2413, Sep. 1977.

[20] B. M. Welsh and S. C. Koeffler, "Remote sensing of atmospheric turbulence and transverse winds from wave-front slope measurements from crossed optical paths," *Appl. Opt.*, vol. 33, no. 21, pp. 4880–4888,1994.

[21] H. Trinqueta, A. Agabia, J. Vernina, M. Azouita, E. Aristidia, and E. Fossat, "Optical turbulence and outer scales above dome C in Antarctica," *Proc. SPIE.*, vol. 7012, pp. 701225-1–701225-8, Jul. 2008.

[22] J. Mchugh and R. Sharman, "Generation of mountain wave-induced mean flows and turbulence near the tropopause," *Quart. J. Roy. Meteorol. Soc.*, vol. 139, no. 675, pp. 1632–1642, 2013.

[23] V. Kornilov, A. Tokovinin, N. Shatsky, O. Voziakova, S. Potanin, and B. Safonov, "Combined MASS-DIMM instruments for atmospheric turbulence studies," *Monthly Notices Roy. Astronomical Soc.*, vol. 382, no. 3, pp. 1268–1278, Nov. 2007.

[24] D. Qin, P. Gian-Kasper, and T. F. Stocker, *Climate Change 2013: The Physical Science Basis, Contribution of Working Group I to the Fifth Assessment Report of the Intergovernmental Panel on Climate Change*. Cambridge, U.K.: Cambridge Univ. Press, 2013.

[25] D. Qin and T. Stocker, "Highlights of the IPCC working group I fifth assessment report," *Adv. Climate Change Res.*, vol. 10, no. 1, pp. 1–6, 2014.

[26] T. Wang, T. Gao, H. Zhang, M. Ge, H. Lei, P. Zhang, P. Zhang, C. Lu, C. Liu, H. Zhang, Q. Zhang, H. Liao, H. Kan, Z. Feng, Y. Zhang, X. Qie, X. Cai, M. Li, L. Liu, and S. Tong, "Atmospheric science study in China in recent 70 years: Atmospheric physics and atmospheric environment," *Special Topic 70th Anniversary Founding People's Republic China, Sci. China Earth Sci.*, vol. 49, pp. 1833–1874, 2019.

[27] S. Yu, Q. Fang, X. Xu, N. Weng, and L. Xiao, "Estimation of Optical turbulence intensity by ultrasonic anemometer," *J. Atmos. Environ. Opt.*, vol. 2, no. 3, pp. 184–187, 2007.

[28] R. Yuan, Z. C. Zeng, and S. Ma, "Estimation optical turbulence by meteorology factor," *Chin. J. Quantum Electron.*, vol. 18, no. 1, pp. 87–91, 2001.

[29] C. Qing, X. Wu, H. Huang, Q. Tian, W. Zhu, R. Rao, and X. Li, "Estimating the surface layer refractive index structure constant over snow and sea ice using Monin–Obukhov similarity theory with a mesoscale atmospheric model," *Opt. Express*, vol. 24, no. 18, pp. 20424–20436,2016.

[30] X. Hu, P. M. Klein, and M. Xue, "Evaluation of the updated YSU planetary boundary layer scheme within WRF for wind 2 resource and air quality assessments," *J. Geophys. Res. Atmos.*, vol. 118, no. 10, pp. 10490–10505, 2013.

[31] S. Chowdhury, J. Zhang, A. Messac, and L. Castillo, "Unrestricted wind farm layout optimization (UWFLO): Investigating key factors influencing the maximum power generation," *Renew. Energy*, vol. 38, no. 1, pp. 16–30, Feb. 2012.

[32] X. Zhai, S. Wu, and B. Liu, "Doppler lidar investigation of wind turbine wake characteristics and atmospheric turbulence under different surface roughness," *Opt. Express*, vol. 25, no. 12, pp. A515–529, 2017.

[33] R. D. Marks, J. Vernin, M. Azouit, J. W. Briggs, M. G. Burton, M. C. B. Ashley, and J. F. Manigault, *Astronomy Astrophys.*, vol. 118, p. 385, 1996.

[34] T. Cherubini and S. Businger, "Another look at the refractive index structure function," *J. Appl. Meteorol. Climatol.*, vol. 52, no. 2, pp. 498–506, Feb. 2013.

[35] C. Qing, X. Wu, X. Li, W. Zhu, C. Qiao, R. Rao, and H. Mei, "Use of weather research and forecasting model outputs to obtain near-surface refractive index structure constant over the ocean," *Opt. Express*, vol. 24, no. 12, pp. 13303–13315, 2016.

[36] N. Weng, Z. Zeng, L. Xiao, C. Ma, and Z. Gong, "Profile and characteristic of refractive index structure constant," *High Power Laser Part. Beams*, vol. 11, no. 6, pp. 673–676, 1999.

[37] S. Y. Shao, X. B. Li, Y. J. Li, W. Y. Zhu, D. Y. Kang, C. Y. Fan, and N. Q. Weng, "Daily variation analysis of atmospheric turbulence from inland to open sea," *J. Phys., Conf. Ser.*, vol. 679, Feb. 2016, Art. no. 012051.

[38] A. M. Obukhov, "Structure of the temperature field in turbulent flows," *Izv Acad Nauk SSSR. Ser. Geograf. Geoz.*, vol. 13, pp. 58–69, 1949.

[39] J. C. Wyngarrd and Y. Izumi, "Behavior of the refractive-index-structure parameter near the ground," *J. Opt. Soc. Amer.*, vol. 61, no. 12, pp. 1646–1650, 1971.

[40] T. Foken and B. Wichura, "Tools for quality assessment of surface-based flux measurements," *Agricult. Forest Meteorol.*, vol. 78, nos. 1–2, pp. 83–105, Jan. 1996.

[41] R. Rao, *Modernized Atmospheric Optics*. Beijing, China: Science Press, 2012, pp. 415–445.

[42] X. Xu, S. Xu, W. X. Wang, and X. Yue, "Design of wireless transmission system based on CC1100," *Sci. Tech. Eng.*, vol. 12, no. 24, pp. 6040–6045, 2012.

[43] L. Li, D. Wang, and J. Zu, "Design of wireless data transmission system based on CC1100," *Res. Develop.*, vol. 26, no. 12, pp. 42–45, 2007.

[44] J. Li, S. Yao, and W. Mi, "Design of the wireless data communication system based on CC1100," *Electron. Test*, vol. 1, pp. 101–104, 2013.

[45] J. gong, M. Liu, H. Wang, F. Yang, J. Tang, and B. Li, "Measurement and analysis of atmospheric coherence length near sea surface," *Opt. Commun. Tech.*, vol. 9, pp. 44–46, 2018.
[46] J. S. Irwin and F. S. Binkowski, "Estimation of the Monin–Obukhov scaling length using on-site instrumentation," *Atmos. Environ.*, vol. 15, no. 6, pp. 1091–1094, Jan. 1981.
[47] A. Venkatram, "Estimating the Monin–Obukhov length in the stable boundary layer for dispersion calculations," *Boundary-Layer Meteorol.*, vol. 19, no. 4, pp. 481–485, Dec. 1980.
[48] B. Figueroa-Espinoza and P. Salles, "Local Monin–Obukhov similarity in heterogeneous terrain," *Atmos. Sci. Let.*, vol. 15, no. 4, pp. 299–306, 2014.
[49] H. Mei, X. Wu, and R. Rao, "Measurement and analysis of temperature power spectrum scaling exponent in non-Kolmogorov turbulent atmosphere," *High Power Laser Part. Beams*, vol. 18, no. 9, pp. 1423–1427, 2006.

SHIYONG SHAO received the B.S. degree in physical education from Liaocheng University, in 2002, the M.S. degree in optics and the Ph.D. degree in atmospheric physics and environment from the Hefei Institutes of Physical Science, Chinese Academy of Sciences, in 2005 and 2009, respectively.

From 2009 to 2011, he was a Research Assistant with the Hefei Institutes of Physical Science, Chinese Academy of Sciences, where he was an Assistant Professor, from 2012 to 2016. Since 2017, he was a Professor at the Hefei Institutes of Physical Science, Chinese Academy of Sciences. He is the author of one books, more than 30 articles, and more than 15 inventions. His research interests include laser atmospheric transmission, development of optical testing equipment, and atmospheric turbulence.

Dr. Shao is a guidance expert in exhaust gas detection and meteorological detection of Qingdao Customs.

FUQIANG QIN received the B.S. degree in mechanical and electrical engineering from Qingdao University, in 2005, and the M.S. degree in computer data processing from Tsinghua University, in 2008. He is currently pursuing the Ph.D. degree with the School of Computer Science and Technology, Northwestern Polytechnical University.

Since 2006, he has been working at Qingdao University. His research interests include big data processing and computer programming.

QING LIU received the B.S. and M.S. degrees in computer engineering from the China University of Petroleum, in 2005 and 2008, respectively. He is currently pursuing the Ph.D. degree with the Hefei Institutes of Physical Science, Chinese Academy of Sciences. His research interest includes development of turbulence measurement equipment and circuit research.

MANMAN XU received the B.S. degree in electrical engineering from Anhui University, in 2017. He is currently pursuing the master's degree with the Hefei Institutes of Physical Science, Chinese Academy of Sciences. His research interests include field test, big data processing, and digital image processing.

XUELING CHENG received the B.S. degree from the School of Aircraft Engineering, Beijing Institute of Technology, in 1993, and the Ph.D. degree from the School of Mechanical and Electrical Engineering, in 1999.

From 1999 to 2003, she held a postdoctoral position at the State Key Laboratory of Turbulence, Peking University, and the Department of Engineering Mechanics, Tsinghua University. Since May 2003, she has been working with the State Key Laboratory of Atmospheric Boundary Layer Physics and Atmospheric Chemistry, Institute of Atmospheric Physics, Chinese Academy of Sciences, where she has been a Professor, since 2017. Her research interests include atmospheric boundary layer physics and atmospheric turbulence theory.

Dr. Cheng won the 2010 (Fifth) Science and Technology Innovation Contribution Award from the Institute of Atmospheric Physics, Chinese Academy of Sciences.